

Article

Drawing-Induced Evolution of Inclusions in Cold-Drawn Pearlitic Steel

Jesús Toribio * , Francisco-Javier Ayaso  and Rocío Rodríguez 

Fracture & Structural Integrity Research Group (FSIRG), Campus Viriato, University of Salamanca (USAL) E.P.S., Avda. Requejo 33, 49022 Zamora, Spain; fja@usal.es (F.-J.A.); rociorg@usal.es (R.R.)

* Correspondence: toribio@usal.es; Tel.: +34-677566723

Abstract: This article focuses on the analysis of the evolution of inclusions present in eutectoid pearlitic steel subjected to a real cold drawing process. To this end, wires belonging to different stages of the manufacture chain were studied, starting from an initial hot rolled bar (not cold drawn at all). In addition to the information obtained through visual inspection, a quantitative analysis of the microdefects generated by these inclusions was carried out. The analysis was performed using materialographic techniques, scanning electron microscopy (SEM) and the image analysis program (AnaliSYS 3.1[®]).

Keywords: pearlitic steel; inclusions; cold drawing



Citation: Toribio, J.; Ayaso, F.-J.; Rodríguez, R. Drawing-Induced Evolution of Inclusions in Cold-Drawn Pearlitic Steel. *Metals* **2021**, *11*, 1272. <https://doi.org/10.3390/met11081272>

Academic Editor: Ildiko Peter

Received: 30 June 2021

Accepted: 9 August 2021

Published: 12 August 2021

Publisher's Note: MDPI stays neutral with regard to jurisdictional claims in published maps and institutional affiliations.



Copyright: © 2021 by the authors. Licensee MDPI, Basel, Switzerland. This article is an open access article distributed under the terms and conditions of the Creative Commons Attribution (CC BY) license (<https://creativecommons.org/licenses/by/4.0/>).

1. Introduction

The inclusions present in steel have been the subject of many scientific studies, focusing mainly on their composition, size and morphology [1–4]. Some of the studies deal with the spatial distribution and shape of inclusions using mathematical modelling, using the method called shape control [5]. In pearlitic steels, a multitude of inclusions has been observed, among which oxides, silicates, manganese sulfides, carbides and also, to a lesser extent, nitrides stand out [6]. As for the progressively drawn pearlitic steels, subject of study in the present work, the influence of the inclusions on the anisotropic behavior in fracture has been recently analyzed [7].

Some researchers have studied the influence of inclusions on the initiation of cracks generated by fatigue in pearlitic steels, analyzing the morphology and distribution of these inclusions [8–11]. The scientific literature includes numerous studies focused on the quantification of morphology and its subsequent classification, using dispersive energy spectroscopy techniques [12,13]. The most recent research deals with the analysis of the different types of inclusions and their influence on the mechanical properties of steel [14–17]. It is worth mentioning the studies focused on improving the deformability of fragile inclusions in order to ensure a good mechanical performance of the steel during the drawing process [18,19], or the modification of the process itself, hot rolling, to obtain inclusions that improve the final mechanical properties of the steel [20].

The cold drawing process causes microstructural changes in the steel, such as the reorientation of the perlite colonies and the lamellae that make them up (ferrite and cementite) in the direction of the longitudinal wire axis, a progressive decrease in the interlaminar spacing and an increase in the slenderness of the colonies [21,22].

In pearlitic steel, the greatest addition of alloying substances occurs to promote or enhance the nucleation of perlite. Some studies try to analyze, by means of isothermal methods, the influence of inclusions on the nucleation of intergranular ferrite in hypoeutectoid steels [23]. The nucleation of non-metallic inclusions of ferrite in steels is different depending on the chemical composition. Experimentally, for medium carbon steels, it was observed that the following compounds are not intergranular ferrite enhancers: SiO₂, MnO-SiO₂, Al₂O₃, TiN and MnS. On the contrary, the inclusions of chemical compositions such

as MnS and Al₂O₃, in steels with a presence of V and N, are enhancers of the nucleation of the intergranular ferrite [24]. The inclusions chemically analyzed in the pearlitic steel wires therefore belong to the group of endogenous or second phase inclusions, which have their origin in alloying substances added to enhance the nucleation of perlite.

The critical size of the inclusion for the creation of microcracks has been well studied [25–27] but generally cannot be concluded at an exact size, as it depends on the type of steel and the characteristics of the inclusion. The critical size of the inclusion has been quantified for tool steels [26], steels AISI 4140 [5], ADF1 [27] (steel produced by Dalian Iron and the CO group based on the chemical composition of commercial steel 42CrMo decreasing the content of O, N, P, S and H, and increasing the content of V and Ti) and for steels used as mechanical springs [28,29]. As for its size, the measurements of the inclusions studied in pearlitic steel yield a size distribution between 1 and 10 µm. Most of the inclusions analyzed in this study are mainly made up of oxides and sulfides. The variation in the elements in the compounds will regulate the characteristics and mechanical behavior of the inclusion [5,26,27].

This article studies the presence and evolution of inclusions throughout a real process of drawing consisting of seven stages, analyzing five of them: the initial one (hot-rolled steel, without drawing), the final one (commercial wire drawing steel) and three intermediate stages of the manufacturing chain. Special attention is paid to the generation and evolution of the microcracks that occurs around the inclusions when the pearlitic steel wire goes through the different dies of drawing; such microcracks can have an influence on the steel's behavior in fracture [7]. The study of the inclusions was carried out from the characterization of the same through the analysis of their chemical composition, as well as a quantitative morphological study.

2. Materials and Methods

In the following study, an eutectoid pearlitic steel belonging to a real wire drawing chain, formed by seven steps of cold drawing, was used. It was analyzed from the initial hot rolled bar (wire which has not been subjected to any step of the drawing process) to the final commercial prestressing wire. The nomenclature used to identify the analyzed wires consists of a letter, which indicates the family of origin of the wire and a representative number of the drawing step to which the wire belongs, 0 being the number for the initial wire rod, 7 for the final product, and numbers from 1 to 6 to identify the wires corresponding to the intermediate steps. The chemical composition of steel family E is shown in Table 1.

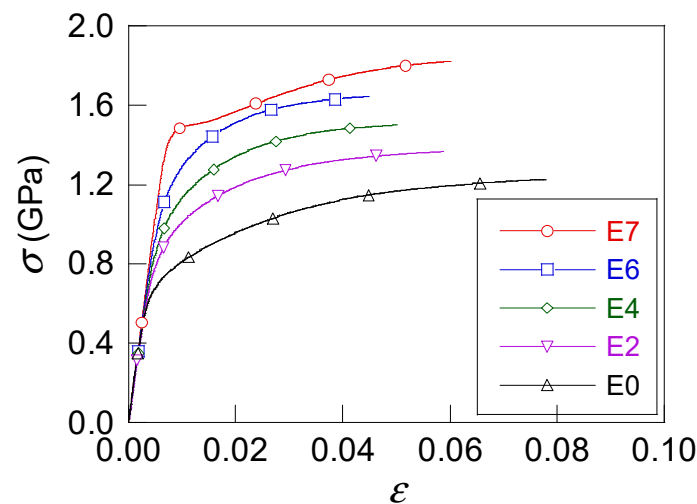
Table 1. Chemical composition (wt.%) of steels of family E (the balance is Fe).

C	Mn	Si	P	S	Al	Cr	V
0.79	0.68	0.21	0.01	0.01	0.003	0.22	0.06

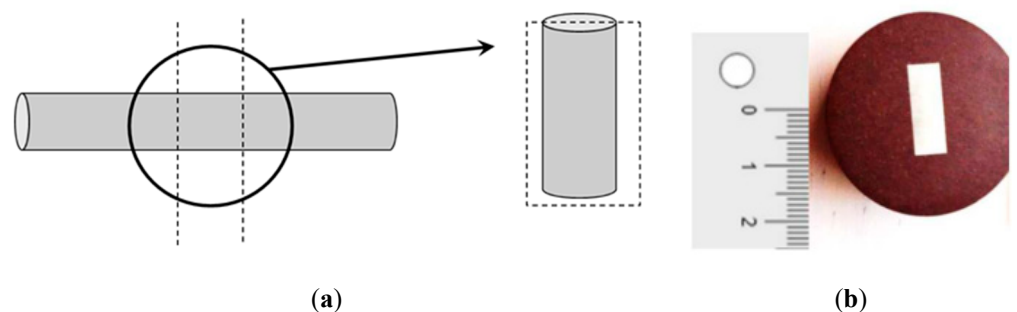
For the study of the evolution of the inclusions in progressively drawn pearlitic steel, the following wires were used: initial hot rolled bar and the wires from the second, fourth, sixth and seventh steps (E0, E2, E4, E6 and E7, respectively) of the cold drawing process. This family of steels has been characterized in previous studies by the Fracture and Structural Integrity Research Group (FSIRG) of the University of Salamanca (USAL) [30], extracting from these the following data indicated in Table 2: the corresponding diameter (D), the plastic deformation [7] that acquires the material at the exit of each corresponding die/stage of the cold drawing process (ϵ_{cum}^P), the Young's modulus (E), the yield stress (σ_Y) and the ultimate tensile stress (σ_R) for each of the wires under study. Figure 1 shows the true stress vs. true deformation curves ($\sigma-\epsilon$) obtained in these studies for all the wires analyzed in the present work.

Table 2. Dimensions and mechanical properties of the steels analyzed.

Steel	D (mm)	ε_{cum}^P	E (GPa)	σ_Y (GPa)	σ_R (GPa)
E0	11.03	0.00	199	0.72	1.23
E2	8.95	0.42	194	0.91	1.36
E4	7.49	0.78	196	1.02	1.50
E6	6.26	1.13	200	1.16	1.62
E7	5.04	1.57	208	1.49	1.83

**Figure 1.** True stress vs. true deformation ($\sigma-\varepsilon$) of steels from family E.

The collection of the samples was carried out with the previous realization of longitudinal cuts in the wires belonging to the different stages of the drawing chain selected, as indicated in the following Figure 2a. This is so that the micrographs of the present work will always be oriented with their vertical side following the cold drawing direction (or the longitudinal wire axis). The sections obtained from the longitudinal cuts (≈ 15 mm long) were rigorously prepared to achieve the correct metallographic observation in the scanning electron microscope (SEM). In order to carry out the micrographs for the study, these sections were embedded in a phenolic resin, thermally hardened by means of a hot compression assembly, as shown in Figure 2b.

**Figure 2.** Preparation of pearlitic steel samples: (a) longitudinal cutting, (b) mounted in resin.

The next step is the execution of the mechanical preparation, grinding and polishing of the samples. This step aims to achieve a specular surface on which a chemical attack can be performed that reveals the microstructure of the corresponding steel. With grinding, which is the first step of the process, a flat surface is achieved (as flat as possible); for this purpose, a turning speed of 300 rpm was used, using water as lubricant, applying a force

of 30 N for 30 s. For the next phase of polishing, three different polishing cloths were used, with 9, 3 and 1 μm diamond powder and applying forces of 30 N for the first two cloths and 20 N for the third one. For all cases, the speed used was 150 rpm and the time was a function of the results obtained in each one. After the mechanical preparation of the samples, a chemical attack with nitric acid (HNO_3) to 3% of solution in pure commercial ethanol was performed. Once the samples were obtained, these were analysed with the scanning electron microscope (SEM) using a JEOL JSM-5610 LV (Jeol Ltd., Tokyo, Japan) in which a multitude of inclusions were visualized in this process; micrographs of said inclusions were made to various scales for further study.

3. Results

The inclusions examined in this study were analyzed using an X-ray dispersion energy analysis unit (EDX, Oxford Instruments, mod. 6587, High Wycombe, UK) coupled to the SEM. The analysis by EDX in the SEM does not determine exactly the statistical composition of the compound that forms the inclusions; however, it identifies the elements that compose them, and provides an approximate information of the percentage of each element that is present in the analyzed inclusion.

Among these inclusions, second phase or endogenous particles were found such as MnS (matte appearance, with irregular shapes), SiO_2 (oxides) and Al_2O_3 (bright appearance and with more regular shapes). The analysis by SEM detected mainly these three types of particles, although others were also found in a smaller proportion and are used for the formation of new phases during the solidification of steel as nucleating agents. The compounds found and analyzed were mainly the following: Ti_2O_3 , Mn silicates (MnOSiO_2 , MnSiO_3), aluminum silicates (SiO_2 , AlO_3), TiN, V and Ca. As a summary, it can be concluded that the inclusions in the steels examined are mainly divided into three distinct groups based on their chemical composition: *sulfides*, *oxides* and *silicates*.

Once the chemical analysis of the inclusions was carried out, it was decided to classify them according to the response to deformation during the drawing process [6], classifying them into *hard*, *soft* and *mix*.

In the first group identified—*hard*-type inclusions—oxides can be found mainly; because of their nature these are usually of high hardness and brittleness; such characteristics prevent them from fully adapting to the surrounding pearlitic matrix during the continuous process of drawing, creating a small discontinuity in the inclusion-pearlite interface (microcavity). As an example, consider Figure 3, which shows a complex oxide embedded in a pearlitic matrix corresponding to an E7 steel, commercial cold drawn pearlitic steel that has passed through seven dies of wire drawing. During the cold drawing, the pearlitic colonies compress the oxide, without breaking it, creating a small inclusion-matrix microcavity during the plastic forming process.

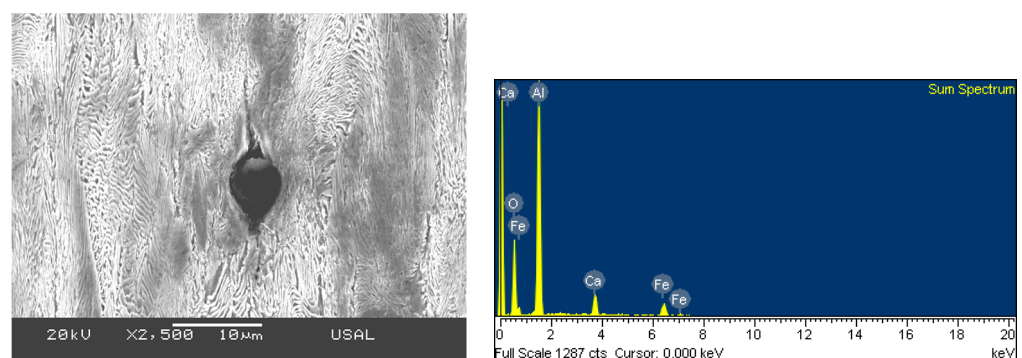


Figure 3. Inclusion of *hard*-type, with complex oxide composition, present in the commercial pre-stressed wire E7.

In the second group of inclusions identified, are those formed mainly by manganese sulfide. Manganese sulfides are capable of withstanding greater plastic deformation than inclusions composed of oxides; however, in many cases they break as a consequence of the cold drawing process, and it is possible to distinguish the parts in which the embedded inclusion has fragmented. Figure 4 shows a *soft*-type inclusion consisting mainly of manganese sulfide. The inclusion and its pearlitic matrix have gone through two dies of wire drawing (E2 steel). It can be observed that the inclusion adapts quite well to the deformation acquired by its matrix during the cold drawing and that it has fragmented during the aforementioned process.

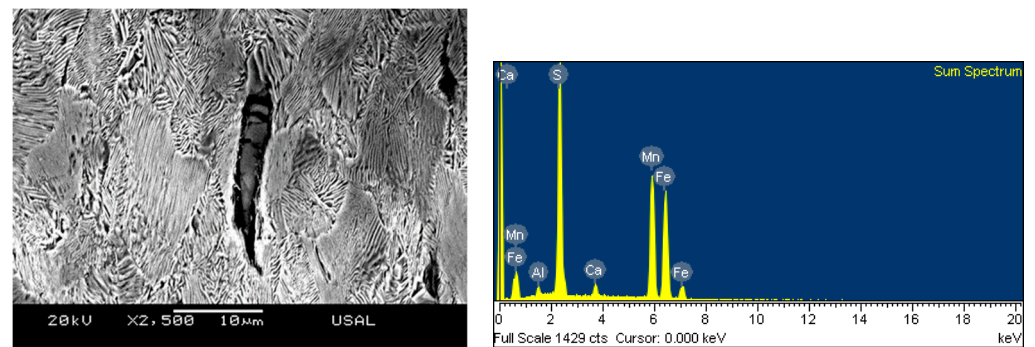


Figure 4. Inclusion of *soft*-type, with main composition of manganese sulfide, belonging to the E2 steel (second drawing step).

It should be noted that in the study carried out, a particular type of inclusions were analyzed, which are formed simultaneously by the two main types of constituents discussed above: oxides and manganese sulfides. These inclusions were called *mix*-type (see Figure 5) and in them it is possible to differentiate an inner part formed by a complex oxide and an outer part, that surrounds this first one, composed mainly by manganese sulfides. The mechanical behavior that these inclusions exhibit, during the cold drawing process, is similar to that of the *soft*-type inclusions, because the outer part of the *mix*-type inclusions (that in direct contact with the surrounding pearlitic matrix) is the *soft* one (oxides on the inside, sulfides on the outside).

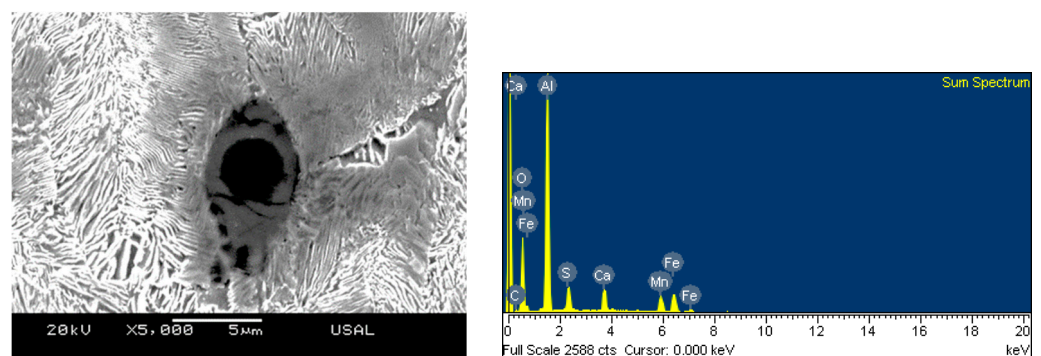


Figure 5. Inclusion of *mix*-type class, with complex oxide composition in the inner central zone and manganese sulfide in the outer zone, present in the initial wire rod E0.

The classification of inclusions in *hard*, *soft* and *mix* obey to their mechanical behavior during the drawing process, a process thanks to which the ferrite and cementite lamellas that make up the pearlite colonies are re-oriented and stretched [21]. The microstructural reorganization of the drawing process produces, in the *soft*-type inclusions, large strains along the longitudinal wire axis (direction of the drawing process); making it able to increase its slenderness by an order of magnitude. In the *hard*-type inclusions, no variation

in their morphology and size was observed; however, microflaws or microcavities around them were observed in the wires belonging to the last steps of the drawing process (see Figure 4) [7]. To quantify the present percentage of the different types of inclusions in steel, measurements were made of a sample composed of 840 of them, extracting the following results (Figure 6).

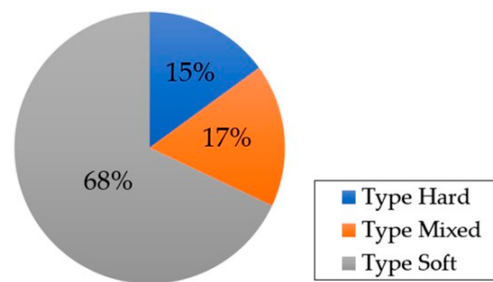


Figure 6. Proportional quantitative results of the different types of inclusions present in steel E.

Once the micrographs were obtained and selected according to the type of inclusion, they were measured using the image analysis program AnaliSYS. 3.1[®]. In order to study the variation in the shape factor of the inclusions throughout the drawing process, the morphology of the inclusion has been approximated to an ellipse. In this way, the major axis ($2a$), parallel to the drawing direction, represented in Figure 7, was measured in the inclusions.

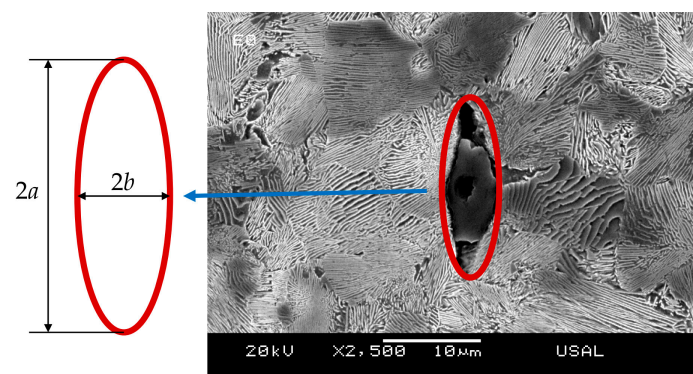


Figure 7. Approximation of the inclusion and its microcavity to an ellipse.

For the measurement of this ellipse axis in the different micrographs it proceeded to measure the inclusion's surface plus the microcavity, or microdamage, generated by it during the cold drawing process. With this surface and the measurement of the major axis of the ellipse, $2a$, the minor axis is obtained using the following equation:

$$S = \pi \cdot a \cdot b \quad (1)$$

where a and b are the semi-axis of the ellipse and S is the inclusion surface or, in the case of non-matching, the surface of the inclusion and the microdamage generated around it. The study of this work focuses on the surface of the microdefect generated or around the inclusion due to the drawing process. Once this data is obtained, it is possible to calculate the shape factor of the inclusions (a/b), making the mean and the standard deviation of the different shape factors obtained in the different steps of the plastic conformation process.

For the inclusions in which there was a decohesion of the pearlitic matrix due to the process of drawing, the surface of microcavity generated was measured (S), which includes the inclusion itself. In those inclusions in which the pearlite–inclusion interface remains united (without detachment from the pearlitic matrix during drawing), only the surface of

the proper inclusion was measured, since it coincides with the value of the surface of the resulting microdamage itself. The shape factor average values for the different inclusions (*hard*, *soft* and *mix*) are shown in the following Figures 8–10. In order to be able to compare these measures, a statistical treatment of the data obtained was carried out, the standard deviation, not being greater than 2 in any case.

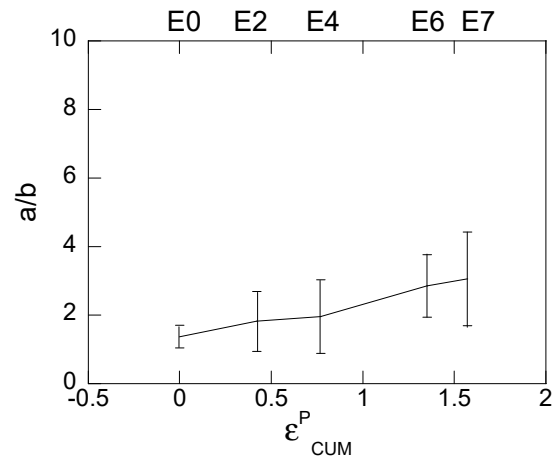


Figure 8. Shape factor evolution for *hard*-type inclusions.

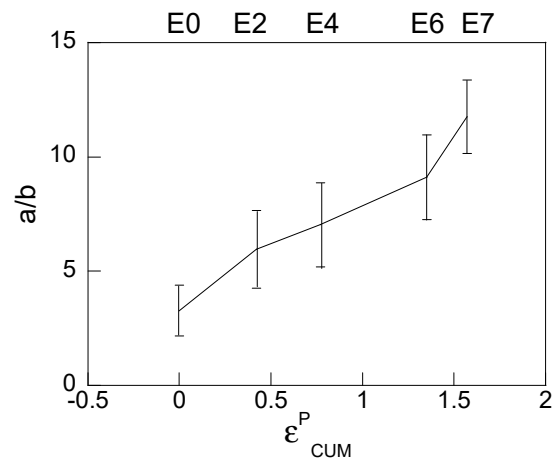


Figure 9. Shape factor evolution for *soft*-type inclusions.

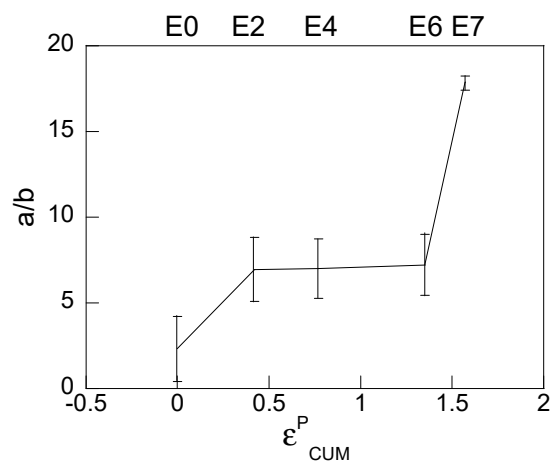


Figure 10. Shape factor evolution for *mix*-type inclusions.

In the micrographs belonging to the initial hot rolled bar steel E0, it is possible to observe inclusions with deformations prior to drawing that can be attributed to the process of hot rolling [14] original steel itself. Figure 8 shows an evolution of the shape factor of the *hard*-type inclusions and the microdamage that they promote. The *hard*-type inclusions, being more resistant than the pearlitic matrix that surrounds them, increase their slenderness a bit during cold drawing due to the generation of microflaws oriented in the direction of the longitudinal wire axis (cold drawing direction).

The *soft*-type inclusions and the microcavities generated by them behave in the same way as the *hard* ones, increasing their slenderness throughout the process; however, this increase is more accentuated in the *soft* ones. Figure 9 shows much greater increases in the shape factor than in the *hard* inclusions.

For the case of *mix*-type inclusions (Figure 10) a similar behavior to the two types of inclusions above mentioned is observed, that is: a progressive increase in their slenderness due to the drawing process. This increase is very similar to that of *soft*-type inclusions, a result which could be expected since the inclusion in contact with the pearlitic matrix is a *soft*-type of inclusion.

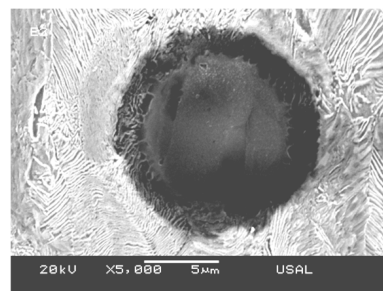
4. Discussion

The distribution of the inclusions is a parameter that is of vital importance in order to understand the mechanical and fracture behavior of steels. The following diagrams of Figures 11–13 show the evolution of the microdamage generated by the inclusions during the drawing process. It can be observed, regardless of the proper nature of the inclusions (*hard*, *soft* and *mix*), how microflaws or microcracks are generated that will be, or not, filled later by the pearlitic matrix surrounding the passage through to several drawing dies. It can be observed how, as the process of drawing progresses, the surrounding pearlitic matrix detaches from the inclusion, generating a kind of microflaw around the considered inclusion; these microcavities are oriented in the direction of the drawing process. Consequently, it can be concluded that they are a consequence of the drawing process. The major axis average values ($2a$, Figure 7) of the measured ellipse can be considered as a quantitative measure of the generated microdamage during cold drawing and due to the presence of the inclusions, i.e., a microcrack oriented in the longitudinal wire axis with a length $2a$. The average value is lower ($2a = 6.17 \mu\text{m}$) for the initial hot rolled steel (E0, not cold drawn at all), and greater ($2a = 17.67 \mu\text{m}$) for those steels corresponding to the last steps of the cold drawing process.

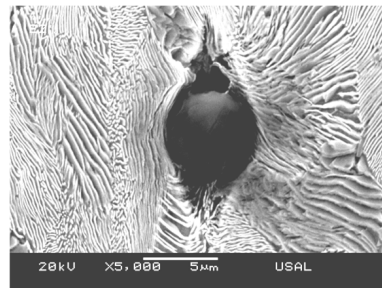
The *hard* inclusions (Figure 11) are not able to undergo the same plastic deformation as the pearlitic matrix that surrounds them during the drawing process. The difference in mechanical behavior between the pearlitic matrix and the inclusion will cause a decohesion of the pearlitic matrix, generating a microflaw, also called microdamage, around it [6,7]. As the drawing process goes ahead, these microdefects tend to deform in the direction of the longitudinal axis of the wire. However, the constraint suffered by the neighboring pearlitic colonies causes the closure of the afore-said colonies. The microdamage generated cause a discontinuity in the material that can subsequently influence the fracture behavior of the steel [7], because they act in a similar way to stress concentrators. Oxides, carbides and nitrides are part of the inclusions that shown this behavior during the cold drawing process.

On the other hand, there are *soft*-type inclusions (Figure 12) which are able to deform plastically in a similar way to the pearlitic matrix that surrounds them during cold drawing; these evolve along all the stretching dies, deforming a lot according to the longitudinal axis of the steel wire (drawing direction). This type of inclusions, once deformed, tend to fragment, generating cavities that will simultaneously be filled by the compression of the surrounding pearlitic matrix when passing through successive drawing dies. Manganese sulfides are one of the most representative compounds of this type of inclusions. Most inclusions will generate microdefects of greater entity the larger the size of that inclusion. The microflaws generated by the *soft*-type inclusions are surrounded by a pearlitic matrix

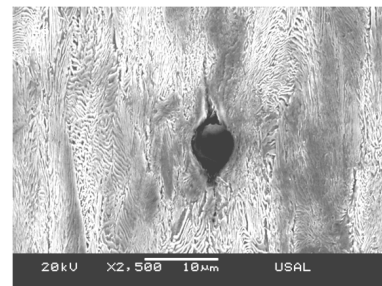
with a large microdamage, that microdamage being of a smaller size than the one generated by other inclusions.



(a)



(b)



(c)

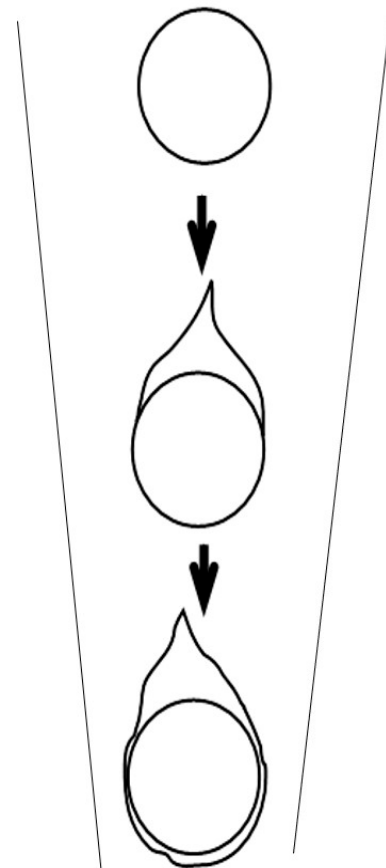
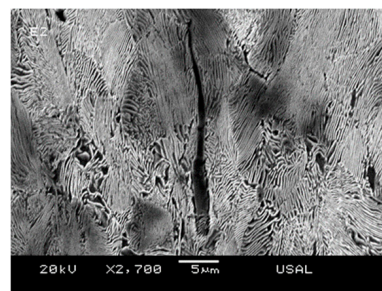


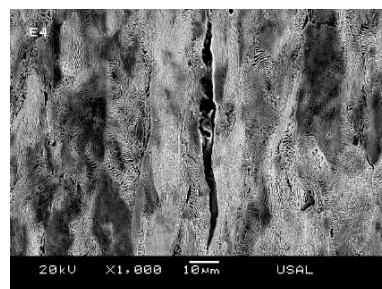
Figure 11. Micrographs and outline of the evolution of *hard*-type inclusions during the drawing process belonging to the steels E2 (a), E4 (b) and E7 (c).

Mix-type inclusions are made up of two typologies of inclusions, one softer and one harder. Both typologies, within the same inclusion, are clearly different by tonality and shape; the *hard*-type inclusion being darker and with a rounded morphology. A multitude of *mix*-type inclusions was observed in the steels studied. In the following diagram—and micrographs (Figure 13)—it is shown how the hardest inclusion appears in the central area of the *mix*-type inclusion, while its periphery is formed by a softer inclusion (of lighter tonality). The microcavity generated from this type of inclusion has a slenderness similar to that generated by the *soft*-type inclusion. The width of this microdamage is greater than that created by *soft*-type inclusion, since the inclusion of *hard*-type existing in the core of the *mix*-type inclusions is barely deformed transversely throughout the drawing process.

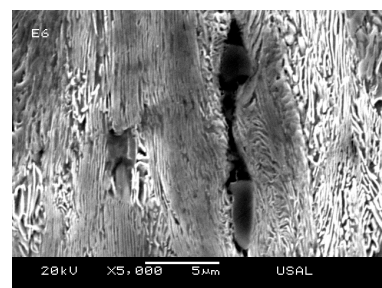
The soft outer part of the *mix*-type inclusion is deformed during the first steps of the drawing process in the direction of the conformation process itself (longitudinal axis of the wire). As this process grows, the soft part of the inclusion can become fragmented forming empty spaces between the different fragments created during drawing. Once the soft part of the *mix*-type inclusion is fragmented, due to the constraint of the colonies during drawing, this area can be filled with the surrounding pearlitic matrix thanks to the constricting action that occurs during drawing. This filling can leave the fragments of the inclusion isolated; this is shown in the micrographs as independent inclusions, but within the same microcavity. As a final result of the process, *mix*-type inclusions generate discontinuities within the pearlitic matrix since the padding is not strictly complete at the edges of the fragments.



(a)



(b)



(c)

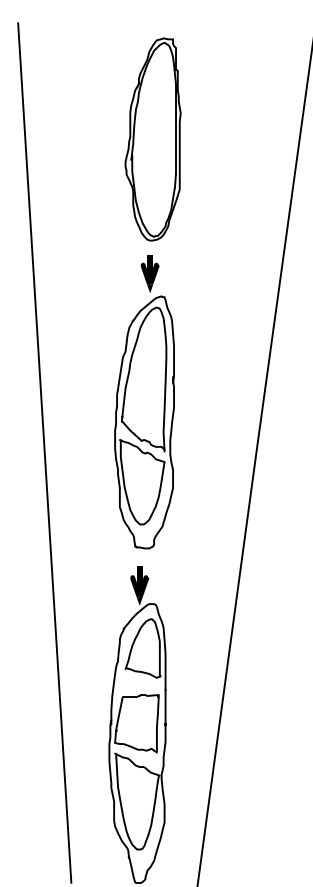


Figure 12. Micrographs and outline of the evolution of the inclusions of *the soft-type* during the drawing process belonging to the steels E2 (a), E4 (b) and E6 (c).

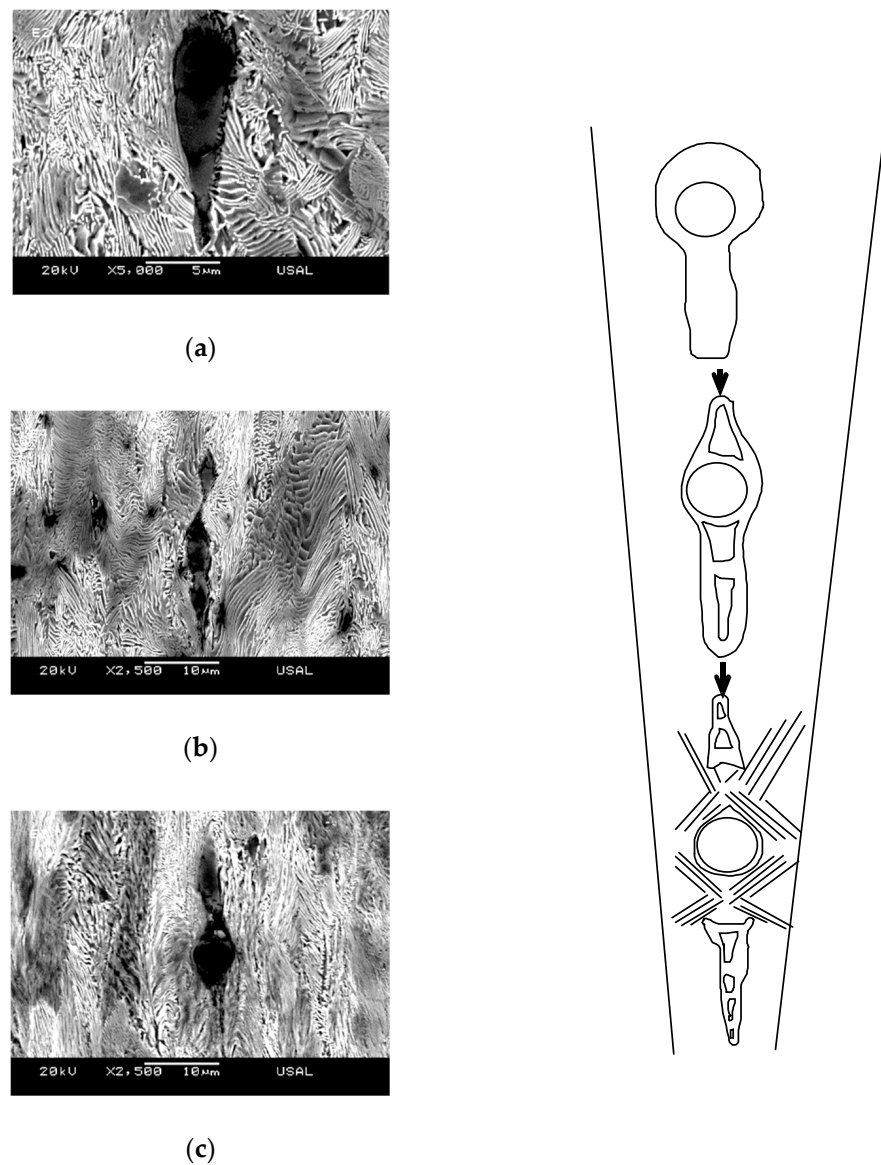


Figure 13. Micrographs and outline of the evolution of the inclusions of the *mix*-type during the drawing process belonging to steels E2 (a), E4 (b) and E6 (c).

5. Conclusions

In this article, a qualitative and quantitative analysis of the inclusions existing in a pearlitic eutectoid steel was performed, paying special attention to the morphological changes in the microdefects generated by the inclusions during the drawing process that suffers the wire during its manufacturing.

The inclusions present in the analyzed pearlitic steel show as main chemical compositions: complex oxides, manganese sulfides, carbides and nitrides.

The classification of the inclusions was carried out, on the other hand, based on their behavior against the surrounding pearlitic matrix during the drawing process. This classification consists of the following: *soft*-type inclusions (mainly MnS type), *hard*-type inclusions (Fe complex oxides) and *mix*-type inclusions (Mn sulfides and iron oxides) in which a *hard*-type inclusion is usually surrounded by a *soft*-type inclusion.

As for the percentages of distributions of the analyzed inclusions, it can be concluded that there is a greater proportion of *soft*-type inclusions (68%), while the remaining percentage of inclusions found is distributed as follows: *hard*-type (15%) and *mix*-type (17%).

The existing inclusions in the steel, as it passes through the various wire drawing dies, generate a series of microflaws elongated in the longitudinal direction of the steel wire. These microflaws or microdamage show an increase in their slenderness (parallel to the direction of the plastic conformation process, or longitudinal axis of the wire) as a consequence of the drawing process itself; such increase being more pronounced in the case of *soft*-type inclusions. In the transverse direction to the steel wire, the material becomes compacted by diametral compression of the wire when it passes through the different cold drawing dies.

The volume of the microdamage generated around an inclusion during cold drawing is a function, fundamentally, of the size of the inclusion from which it originates, of the chemical composition of the inclusion and of the number of dies of drawing which has exceeded the corresponding inclusion (and its wire).

The presence of inclusions within the microstructure of pearlitic steel, as well as the microdamage that occur around them as an exclusive consequence of the drawing process, can be key to understanding the mechanical response of the material and also its fracture behavior.

Author Contributions: J.T. conceived and designed the research; F.-J.A. and R.R. performed the microscopy analysis, J.T., F.-J.A. and R.R. analyzed the data and wrote the paper. All authors have read and agreed to the published version of the manuscript.

Funding: This research was funded by the following Spanish Institutions: Ministry for Science and Technology (MICYT; Grant MAT2002-01831), Ministry for Education and Science (MEC; Grant BIA2005-08965), Ministry for Science and Innovation (MICINN; Grant BIA2008-06810), Ministry for Economy and Competitiveness (MINECO; Grant BIA2011-27870) and Junta de Castilla y León (JCyL; Grants SA067A05, SA111A07, SA039A08 and SA132G18).

Institutional Review Board Statement: Not applicable.

Informed Consent Statement: Not applicable.

Data Availability Statement: Not applicable.

Conflicts of Interest: The authors declare no conflict of interest. With regard to the research funds, the different institutions providing financial support for the scientific research had no role in the design of the study; in the collection, analyses, or interpretation of data; in the writing of the present manuscript; and in the decision to publish the results.

References

1. Yan, J.; Li, T.; Shang, Z.; Guo, H. Three-Dimensional Characterization of MnS Inclusions in Steel during Rolling Process. *Mater. Charact.* **2019**, *158*, 109944. [[CrossRef](#)]
2. Atkinson, H.V.; Shi, G. Characterization of Inclusions in Clean Steels: A Review Including the Statistics of Extremes Methods. *Prog. Mater. Sci.* **2003**, *48*, 457–520. [[CrossRef](#)]
3. Luo, C.; Stahlberg, U. Deformation of Inclusions during Hot Rolling. *J. Mater. Process. Technol.* **2001**, *114*, 87–97. [[CrossRef](#)]
4. Wilson, A.D. The Influence of Thickness and Rolling Ratio on the Inclusion Behavior in Plate Steels. *Metallography* **1979**, *12*, 233–255. [[CrossRef](#)]
5. Collins, S.R.; Michal, G.M. Inclusion Engineering for Improved Fatigue Response in Forged AISI 4140 Steel. In Proceedings of the Conference High Performance Structural Steels, Cleveland, OH, USA, 29 October–2 November 1995; pp. 269–280.
6. Rodríguez, R. Daño Microestructural Producido Durante la Fabricación de Aceros de Pretensado y Consecuencias en su Comportamiento en Fractura. Ph.D. Thesis, University of Salamanca, Salamanca, Spain, 2008.
7. Toribio, J.; Ayaso, F.J.; González, B. Role of Non-Metallic Inclusions in the Fracture Behavior of Cold Drawn Pearlitic Steel. *Metals* **2021**, *11*, 962. [[CrossRef](#)]
8. Liu, C.D.; Bassim, M.N.; Lawrence, S. Evaluation of Fatigue-Crack Initiation at Inclusions in Fully Pearlitic Steels. *Mater. Sci. Eng.* **1993**, *167*, 107–113. [[CrossRef](#)]
9. Schäfer, B.J.; Sonnweber-Ribic, P.; Hassan, H.; Hartmaier, A. Micromechanical Modeling of Fatigue Crack Nucleation around Non-Metallic Inclusions in Martensitic High-Strength Steels. *Metals* **2019**, *9*, 1258. [[CrossRef](#)]
10. Cong, T.; Qian, G.; Zhang, G.; Wu, S.; Pan, X.; Du, L.; Liu, X. Effects of Inclusion Size and Stress Ratio on the Very-High-Cycle Fatigue Behavior of Pearlitic Steel. *Int. J. Fatigue* **2021**, *142*, 105958. [[CrossRef](#)]
11. Li, Z.; Zhou, S.; Yang, C.; Yong, Q. High/Very High Cycle Fatigue Behaviors of Medium Carbon Pearlitic Wheel Steels and the Effects of Microstructure and Non-Metallic Inclusions. *Mater. Sci. Eng.* **2019**, *764*, 138208. [[CrossRef](#)]

12. Kang, Y.B.; Kim, H.S.; Zhang, J.; Lee, H.E. Practical Application of Thermodynamics to Inclusions Engineering in Steel. *J. Phys. Chem. Solids* **2005**, *66*, 219–225. [[CrossRef](#)]
13. Mainy, D. Morphological and Analytical Characterization of Inclusions: Relation with Processing Parameters and Properties of Use. *Mater. Charact.* **2003**, *36*, 321–326. [[CrossRef](#)]
14. Yu, H.; Bi, H.; Liu, X.; Chen, L.; Dong, N. Behavior of Inclusions with Weak Adhesion to Strip Matrix During Rolling using FEM. *J. Mater. Process. Technol.* **2009**, *209*, 4274–4280. [[CrossRef](#)]
15. Ånmark, N.; Karasev, A.; Jönsson, P.G. The Effect of Different Non-Metallic Inclusions on the Machinability of Steels. *Materials* **2015**, *8*, 751–783. [[CrossRef](#)] [[PubMed](#)]
16. Guo, J.; Yang, W.; Shi, X.; Zheng, Z.; Liu, S.; Duan, S.; Wu, J.; Guo, H. Effect of Sulfur Content on the Properties and MnS Morphologies of DH36 Structural Steel. *Metals* **2018**, *8*, 945. [[CrossRef](#)]
17. Qiu, G.; Zhan, D.; Li, C.; Yang, Y.; Qi, M.; Jiang, Z.; Zhang, H. Influence of Inclusions on the Mechanical Properties of RAFM Steels Via Y and Ti Addition. *Metals* **2019**, *9*, 851. [[CrossRef](#)]
18. Yan, W.; Xu, H.C.; Chen, W.Q. Study on Inclusions in Wire Rod of Tire Cord Steel by Means of Electrolysis of Wire Rod. *Steel Res. Int.* **2014**, *85*, 53–59. [[CrossRef](#)]
19. Yan, W.; Chen, W.; Li, J. Quality Control of High Carbon Steel for Steel Wires. *Materials* **2019**, *12*, 846. [[CrossRef](#)]
20. Liu, H.; Hu, D.; Fu, J. Analysis of MnS Inclusions Formation in Resulphurised Steel via Modeling and Experiments. *Materials* **2019**, *12*, 2028. [[CrossRef](#)]
21. Toribio, J.; Ovejero, E. Microstructure Evolution in a Pearlitic Steel Subjected to Progressive Plastic Deformation. *Mater. Sci. Eng.* **1997**, *234–236*, 579–582. [[CrossRef](#)]
22. Toribio, J.; Ovejero, E. Microstructure Orientation in a Pearlitic Steel Subjected to Progressive Plastic Deformation. *J. Mater. Sci. Lett.* **1998**, *17*, 1037–1040. [[CrossRef](#)]
23. Pan, T.; Yang, Z.G.; Zhang, G.; Bai, B.Z.; Fang, H.S. Kinetics and Mechanisms of Intragranular Ferrite Nucleation on Non-Metallic Inclusions in Low Carbon Steels. *Mater. Sci. Eng.* **2006**, *438–440*, 1128–1132. [[CrossRef](#)]
24. Shim, J.H.; Oh, Y.J.; Suh, J.Y.; Cho, Y.W.; Shim, J.D.; Byum, J.S.; Lee, D.N. Ferrite Nucleation Potency of Non-Metallic Inclusion in Medium Carbon Steels. *Acta Mater.* **2001**, *49*, 2115–2122. [[CrossRef](#)]
25. Zhang, J.M.; Zhang, J.F.; Yang, Z.G.; Li, G.Y.; Yao, G.; Lia, S.X.; Hui, W.J.; Weng, W.J. On the Critical Inclusion Size of High Strength Steels under Ultra-High Cycle Fatigue. *Mater. Sci. Eng.* **2006**, *427*, 167–174.
26. Meurling, F.; Melander, A.; Tidesten, M.; Westin, L. Influence of Carbide and Inclusion Contents on the Fatigue Properties of High Speed Steels and Tool Steels. *Int. J. Fatigue* **2001**, *23*, 215–224. [[CrossRef](#)]
27. Zhang, J.M.; Zhang, J.F.; Yang, Z.G.; Li, G.Y.; Yao, G.; Lia, S.X.; Hui, W.J.; Weng, W.J. Estimation of Maximum Inclusion Size and Fatigue Strength in High-Strength ADF1 Steel. *Mater. Sci. Eng.* **2005**, *394*, 126–131. [[CrossRef](#)]
28. Zhang, J.M.; Li, X.S.; Yang, Z.G.; Li, G.Y.; Hui, W.J.; Weng, Y.Q. Influence of Inclusion Size on Fatigue Behavior of High Strength Steels in the Gigacycle Fatigue Regime. *Int. J. Fatigue* **2006**, *29*, 765–777. [[CrossRef](#)]
29. Chapetti, M.D.; Tagawa, T.; Miyata, T. Ultra-Long Cycle Fatigue of High-Strength Carbon Steels Part II: Estimation of Fatigue Limit for Failure from Internal Inclusions. *Mater. Sci. Eng.* **2003**, *356*, 236–244. [[CrossRef](#)]
30. Toribio, J.; Ayaso, F.-J.; González, B.; Matos, J.-C.; Vergara, D.; Lorenzo, M. Tensile Fracture Behavior of Progressively-Drawn Pearlitic Steels. *Metals* **2016**, *6*, 114. [[CrossRef](#)]